Journal of Materials Chemistry C

ROYAL SOCIETY OF CHEMISTRY

PAPER

View Article Online
View Journal | View Issue

Cite this: J. Mater. Chem. C, 2025, 13, 18187

Magnetic-field alignment of micellar lyotropic nematic gels and their memory-effect

Michael Herbst, Max Oliver Dombrowski, Cosima Stubenrauch and Frank Giesselmann *

Received 24th April 2025,
Accepted 4th August 2025

DOI: 10.1039/d5tc01659b

rsc.li/materials-c

Many potential applications of anisotropic hydrogels, such as media for tissue engineering and drug delivery, as well as biomimetic actuators, require gels that are macroscopically aligned over macroscopic length scales. Micellar lyotropic nematic gels, a relatively new class of anisotropic hydrogels, may provide a rather simple and robust approach to macroscopically aligned anisotropic hydrogels if the long-range orientational order of the surfactant-based lyotropic liquid crystal is transferred to the order of the gel network. Here, we report a kinetically controlled process by which we have successfully fabricated centimeter-long sample films of macroscopically aligned nematic gels. This was achieved by growing a self-assembling fibrillar network (SAFIN) of the gelator 3,5 bis (5-hexylcarbamoyl-pentoxy)-benzoate acid hexyl ester (BHPB-6) in a magnetically aligned lyotropic nematic liquid crystal of rod-like micelles formed by the surfactant *N*,*N*-dimethyl-*N*-ethyl-1-hexadecylammonium bromide (CDEAB). Once the gel network is fully formed after typically 10 hours, the macroscopic alignment of the sample is (i) preserved also after removal of the magnetic field and (ii) even recovered after melting and re-forming the nematic liquid crystal. The fibrillar network thus appears to have a remarkable memory-effect that stabilizes the anisotropy of the gel and results in very robust anisotropic hydrogels.

1. Introduction

Among the various examples of lyotropic liquid crystal (LLC) gels, ranging from the long-known lamellar gel phases L_β and $L_{\beta'}$[1,2] to the anisotropic suspensions of percolating rod-shaped nanoparticles,[3–6] micellar LLC gels[7,8] are a relatively new class of liquid crystalline networks that combine two very different structures (Fig. 1(c)–(f)). On the one hand, we have an anisotropic LLC phase consisting of long-range ordered surfactant micelles or bilayers. On the other hand, we have a network of gel fibers. If the gel is a physical gel – as opposed to a chemical gel – its formation and destruction is reversible.[9,10] The gel fibers may consist of polymers such as gelatin[11] or of low molecular weight gelator (LMWG) molecules.[12] In the latter case, the molecules self-assemble *via* non-covalent interactions, inducing one-dimensional fiber growth.[9,12–14] These fibers, in turn, intertwine to form a three-dimensional network called a self-assembled fibrillar network (SAFIN).[15,16] The SAFIN immobilizes the LLC and the resulting LLC gel thus combines the anisotropy of a micellar LLC with the mechanics of a physical gel. These new micellar LLC gels provide relatively easy and versatile access to macroscopically anisotropic hydrogels, but the first example of a micellar nematic LLC gel was not reported before 2021.[17] For the sake of simplicity, when we refer to "nematic LLC gels" in the following, we mean precisely these physical gels consisting of a SAFIN and a micellar nematic LLC consisting of rod- or disc-shaped surfactant micelles in water.

Anisotropic hydrogels are becoming increasingly important because of their potential use in biomedical applications.[18] Some surfactant-based lyotropic liquid crystalline structures even occur naturally in biological systems, such as the cell membrane.[19] It is therefore obvious that they can be used to deliver drugs or to embed proteins. As regards the gel, a physical gel has a decisive advantage over a chemical gel because it can be destroyed or formed on demand by changing *e.g.* the concentration, the pH, or the temperature.[20–22] In addition to biomedical applications, LLC gels are, in a sense, also the lyotropic counterparts of thermotropic liquid crystalline elastomers (LCE),[23,24] which became the workhorse for biomimetic actuators and soft robotics.[25–27] In both cases, a change in the macroscopic shape of the network is necessary in response to a phase transition of the enclosed liquid crystal that is triggered by external stimuli.[28–30]

Unlike thermotropic liquid crystals (TLCs), which are relatively easy to align using electric and magnetic fields or rubbed surfaces,[25] the macroscopic alignment of LLC samples is more challenging. This difference is due to the fact that the building blocks of LLCs are micelles in an isotropic solvent, whereas in TLCs the building blocks are single molecules.[31,32] For the alignment of LLC phases several approaches were developed:

Institute of Physical Chemistry, University of Stuttgart, 70569 Stuttgart, Germany. E-mail: f.giesselmann@ipc.uni-stuttgart.de

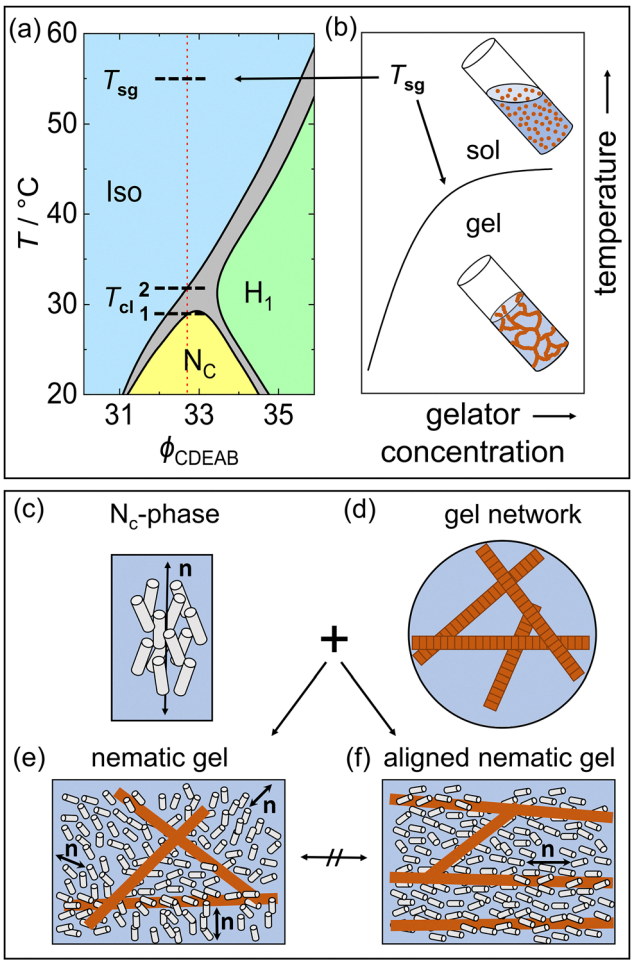

Fig. 1 (a) Temperature dependent phase diagram of the binary system water and surfactant *N*,*N*-dimethyl-*N*-ethyl-1-hexadecylammonium bromide (CDEAB) as function of the surfactant mass fraction ϕ_{CDEAB}. Shown are the nematic phase (N_C), the isotropic phase (Iso), and the hexagonal phase (H_1) with two-phase regions between the phases. The dotted red line indicates the surfactant mass fraction used in this study. The clearing of the N_C-phase is from T_{cl1} = 29 °C to T_{cl2} = 32 °C. Redrawn after.[26] (b) Schematic illustration of the sol–gel temperature (T_{sg}) as function of the gelator concentration. Based on.[25] (c) and (d) Schematic illustrations of the N_C-phase (c) and of the SAFIN (d). (e) Combination of a non-aligned N_C-phase and an isotropic gel network. (f) Combination of an aligned N_C-phase and a gel network with a preferential direction, resulting in a macroscopically aligned anisotropic hydrogel. Based on.[27]

the best results so far were obtained by combining magnetic fields and surface interaction.[33–35] The alignment of LLC gels becomes even more challenging since after the gel network has formed, the LLC phase is immobilized and a macroscopic alignment is no longer possible. Thus, the LLC phase must be macroscopically aligned before it becomes immobilized by the gel network. This is a major challenge, particularly if the LLC clearing temperature is below the SAFIN sol–gel temperature.

However, if we were able to obtain a macroscopically aligned LLC before the gel network forms, at least two important questions would emerge: The first question is whether the gel network, when growing in this anisotropic medium, also acquires macroscopic anisotropy (in the sense that, for example, more of its chain segments run parallel to the LLC director than perpendicular to it)? And the second question is, what happens to the anisotropy of the gel network when the LLC loses its anisotropy, for instance by heating above the clearing temperature to the isotropic LLC state? If the gel network likewise loses its anisotropy, we should expect a macroscopic change in the shape of the sample, as required for actuation applications. However, if the network retains its anisotropy, it could serve as a kind of internal memory that restores the alignment of the LLC even without external forces when the LLC is again cooled below its clearing temperature. This would lead to very robust anisotropic hydrogels, the macroscopic alignment of which is stabilized and restored by the gel network as long as the sol–gel temperature has not been exceeded.

In the present study we describe a kinetically controlled process with which we have indeed successfully fabricated macroscopically aligned anisotropic hydrogels which have exceptional properties, including the remarkable memory-effect outlined above. Our lyotropic liquid crystalline system consists of an aqueous solution of the surfactant *N*,*N*-dimethyl-*N*-ethyl-1-hexadecylammonium bromide (CDEAB). In a concentration range of 31 to 34 wt% surfactant and a temperature range of T = 20–29 °C, a calamitic nematic (N_C-phase) phase is formed (Fig. 1(a)). The clearing temperature range of the N_C-phase (T_{cl1} = 29 °C to T_{cl2} = 32 °C) is lower than the sol–gel temperature range (T_{sg1} = 55 °C to T_{sg2} = 78 °C), which, as previously mentioned, is crucial for applications. The sol–gel temperature can be further analyzed as function of the gelator concentration (Fig. 1(b)). The combination of the N_C-phase (Fig. 1(c)) with a SAFIN (Fig. 1(d)) results in a polydomain LLC texture and a random gel network structure (Fig. 1(e)).[33,36] However, as described in the study at hand, we were able to obtain a macroscopically aligned anisotropic hydrogel (Fig. 1(f)).

2. Experimental

2.1. Materials and sample preparation

In this study, we used the surfactant *N*,*N*-dimethyl-*N*-ethyl-1-hexadecylammonium bromide (CDEAB, Merck KGaA, 98%) (Fig. 2(a)) and double distilled water. This surfactant is able to form a lyotropic nematic phase (N_C-phase) consisting of rod-like micelles at room temperature (Fig. 1(a)). The low molecular weight gelator (LMWG) 3,5-bis(5-hexylcarbamoyl-pentoxy)-benzoic acid hexyl ester (BHPB-6) (Fig. 2(b)) was synthesized in collaboration with the Mésini group.[37] Three different gelator mass fractions were used to gel the N_C-phase 1.0, 1.5, and 2.0 wt%, with the gelator mass fraction always referring to the total mass of the sample. All three components were weighed into a screw-cap glass and tightly sealed (Fig. 2(c) and (d)). The mixture was then placed in a thermoshaker (Hettich MHR 23) at T = 130 °C for 10 minutes and afterwards cooled down to room temperature. This procedure was repeated twice to ensure full homogenization. Afterwards the samples were filled into borosilicate capillaries (electron microscopy sciences) with a height of 0.30 mm, width of 3.0 mm and a wall thickness of 0.300 mm. The capillaries were then flame-sealed and again heated to T = 130 °C for homogenization.

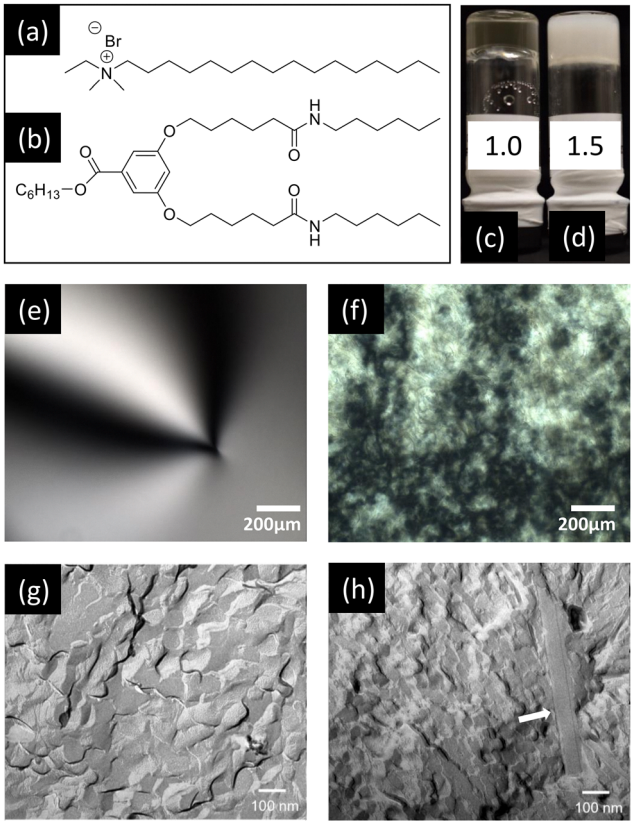

Fig. 2 Chemical structures of the surfactant (a) and the gelator (b) molecules. (c) and (d) Two gelled samples of the nematic N_C-phase, which becomes turbid when the gelator concentration increases from 1.0 to 1.5 wt%. Polarized optical microscope images show a well-developed and characteristic schlieren texture of the nematic LLC (e), and a disturbed schlieren texture for the nematic gel with 1.5 wt% gelator (f). Both samples are encapsulated in flat capillaries (0.3 mm thick). Freeze-fracture electron microscopy (FFEM) images (g) and (h) correspond to the samples in (e) and (f), respectively. A flat gel fiber is clearly visible in the nematic gel (h).

To investigate how the gel network responds to the clearing transition (the transition from the anisotropic nematic to the isotropic phase) of the embedded N_C-phase, the latter should have a clearing temperature range well above room temperature on the one hand and clearly below the sol–gel temperature range (T_{sg1} = 55 °C) on the other. Based on these criteria, we chose a surfactant mass fraction of 32 wt% to water mass fraction 68 wt% such that the resulting N_C-phase transforms into the isotropic phase between T_{cl1} = 29 °C to T_{cl2} = 32 °C. This surfactant mass fraction was kept constant in all our samples. In Fig. 1(a), the composition is indicated by the dashed red line. Unavoidable losses from the evaporation of water cause the effective surfactant concentration to rise slightly by approx. 0.5 to 1.0 wt% during sample preparation. This effect was analyzed for more than 50 samples to obtain a representative value.

2.2. Methods

The samples were examined in transmission by polarized optical microscopy (POM) using a Leica DMLP microscope with a digital camera (Nikon D5300) mounted on the phototube of the microscope. Typical examples of POM images are shown in Fig. 2(e)–(f). While the nematic LLC shows a typical large-scale schlieren texture (Fig. 2(e)) with characteristic half- and integer-numbered singularities (“brushes”), a small-scale and less characteristic polydomain texture is observed in the gelled sample (Fig. 2(f)), which is probably a result of the disturbance of the pristine nematic order by the gel network (Fig. 1(e)).

Freeze fracture electron microscopy (FFEM) was carried out using a Leica EM BAF060 freeze fracture and etching system. The FFEM images in Fig. 2(g) and (h) show a coarse-grained texture indicative of the nematic phase. In the gelled sample (Fig. 2(h)), the gel fiber appears as a flat band embedded within the coarse texture. The observed fiber widths ranged from 22 to 130 nm, with an average width of 46 nm. Mésini *et al.* also described the fiber as flat ribbons,[38] reporting an average ribbon width of 42 nm in cyclohexane.[39]

Time- and temperature-dependent transmission measurements were made by replacing the camera on the phototube of the POM by a photodiode, the photovoltage (proportional to the transmitted light intensity) of which was digitized by a LabJack U12 data acquisition device. The sample temperature was set by a temperature controller (Linkam TMS 94 and LNP 94/2) and a Linkam hot stage mounted on the microscope stage. The LabJack U12 and the Linkam TMS 94 were connected to a computer to control and record automated transmission measurements using a self-written Python script.

For alignment experiments, an electromagnet (Bruker B-E 25v) with power supply (EA-PS 8000 3U) and a magnetic field strength of 1.0 T was used. Samples were placed in a home-made sample holder, the temperature of which was controlled by a temperature controller (JUMO cTRON). A detailed description of the alignment procedure is given in Section 3.2.

3. Results and discussion

3.1. Time-dependent studies on the formation of LLC- and SAFIN structures

In the studied system, as in many other LLC gels, the sol–gel temperature range T_{sg} is above the phase transition temperature range (clearing temperature T_{cl}) from the anisotropic (nematic) to the isotropic micellar phase.[8] When cooling slowly from the sol state below T_{sg}, the SAFIN thus grows in the isotropic micellar phase of the surfactant solution. With further cooling down to T_{cl}, the N_C-phase forms within the already existing gel network. The N_C-phase is thus immobilized by the network from the very beginning and cannot be macroscopically aligned by external force fields. However, the growth of the fibers and the subsequent formation of the fiber network proceeds relatively slowly, often much more slowly than the transformation from the isotropic to the nematic phase. This raises the question of whether very rapid cooling (“quenching”) from the sol state to T_{cl} leaves enough time to align the N_C-phase before the SAFIN has fully formed. To answer this question, we carried out time-dependent (kinetic) thermo-optical investigations in which we can selectively monitor the formation of the LLC phase and the formation of the SAFIN, respectively.

These investigations are based on time- and temperature-dependent transmission measurements using polarized optical microscopy (POM) since the transmission of the nematic gel sample between crossed polarizers is dominated by the optical birefringence of the nematic phase, while the transmission of the same sample without polarizers is determined by the scattering of light at the fiber network and its inhomogeneities. Abrupt changes in sample transmission between crossed polarizers thus clearly indicate the appearance or disappearance of the birefringent liquid crystalline structure.[40] Transmission changes of the sample measured without polarizers indicate the scattering losses due to the formation of the fiber network. Examples of these measurements are shown in Fig. 3 and 4.

Since surfactant-based nematic LLCs are known for their low birefringence,[41,42] the effective optical path difference is small compared to the wavelengths of visible light, and we see greyish first-order interference colors. As a result, the transmission decreases monotonically as the birefringence decreases with temperature and finally reaches a constant minimum value (at least close to zero transmission) in a completely isotropic sample. This allows us to unequivocally monitor the nematic–isotropic phase transition in our samples by means of thermo-optical transmission measurements. Fig. 3(a) shows the temperature dependent transmission of a nematic LLC between crossed polarizers. We start at $T = 25$ °C with a nematic gel that has a polydomain texture whose birefringent nematic domains appear brighter or darker depending on the orientation of their respective director with respect to the polarization plane of the incident light. Overall, the intensity of the transmitted light is high and the sample appears bright. The sample is then heated to $T = 40$ °C at a rate of +1 K min^{-1}. Since the birefringence of a nematic phase decreases slightly and continuously with increasing temperature, the transmission of the sample also decreases slightly upon heating. However, between $T = 32.7$ °C and $T = 34.9$ °C, we observe an abrupt drop in transmission to practically zero. This is the transition of the N_C-phase *via* the corresponding two-phase region into the non-birefringent isotropic micellar phase, which appears completely black between crossed polarizers. After reaching the target temperature of $T = 40$ °C and a certain equilibration time of 5 min, the sample is cooled down to $T = 25$ °C at a rate of −1 K min^{-1}. The N_C-phase returns between $T = 32.8$ °C and $T = 30.1$ °C. Compared to heating, a temperature shift of about 3 °C is observed due to supercooling. However, the corresponding change in transmittance is much less than in the heating run, and the pristine transmittance (prior to heating) is not reached again. The reason for this is the formation of a much finer polydomain texture (see insets in Fig. 3(a)), which has a much darker appearance. However, after a few days of aging and coarsening, the initial texture and transmission are recovered. Overall, from the results shown in Fig. 3(a), we can conclude that the transition from the isotropic to the nematic phase is reversible and takes place within a few minutes.

Fig. 3(b) shows the same experiment, now repeated with the nematic gel containing 1.5 wt% gelator. Even though the measurements in Fig. 3(a) and (b) look very similar, the absolute transmissions differ significantly. The transition now takes place between 32.2 °C and 34.3 °C and is only slightly shifted to lower temperatures by the presence of the network. During the cooling cycle, the nematic phase begins to reappear at 34.3 °C, with practically no supercooling, and is fully returned around three minutes later at 31.1 °C. In addition, the pristine transmission (prior to heating) is almost fully restored and the corresponding textures of the nematic gels (see insets in Fig. 3(b)) are almost identical with more or less all details of the pristine nematic texture being exactly reproduced after the return from the

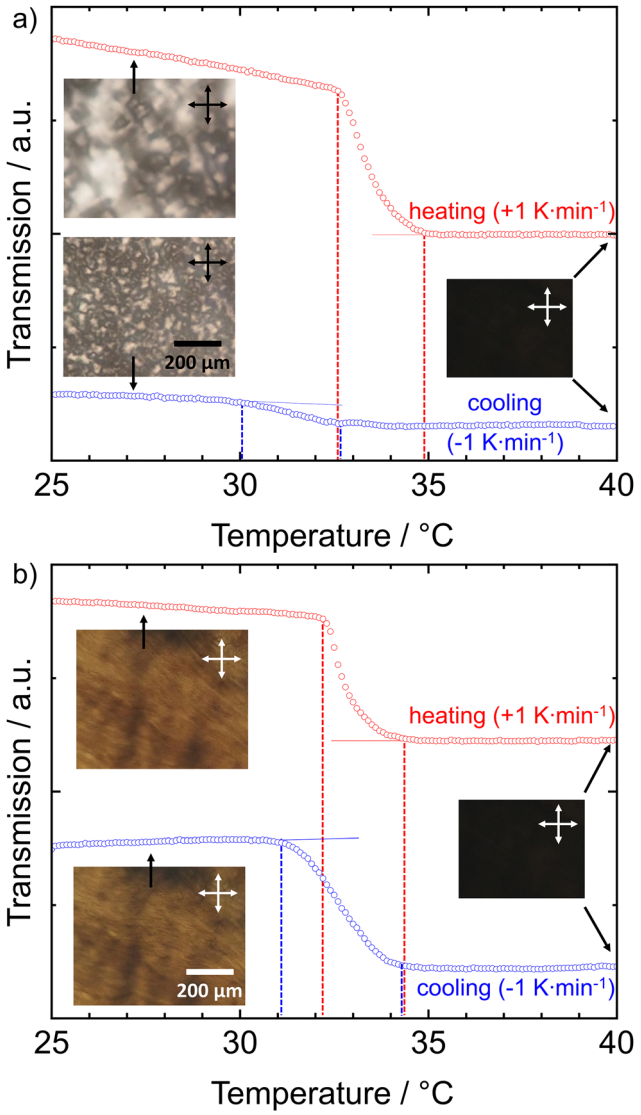

Fig. 3 Thermo-optical measurements of sample transmission between crossed polarizers *vs.* temperature during time-linear heating (red curves) and cooling (blue curves) of (a) the nematic LLC and (b) the nematic gel. Abrupt changes in the slopes of these curves indicate the transition temperature ranges between the birefringent nematic (high transmission) and the non-birefringent isotropic states (low transmission), see the dashed vertical lines. Note that the absolute transmission differs strongly between (a) and (b), and the heating and cooling curves are vertically shifted to each other for better visualization. Thin extrapolation lines are guides to the eye. Insets show the corresponding texture images in the POM.

isotropic state. Apparently, the gel network has some kind of restoring effect which does not exist in the case of the nematic LLC sample in Fig. 3(a). This observation will be revisited and further investigated in Section 3.3.

Fig. 4 shows the results of the temperature quenching experiments to investigate the kinetics of the SAFIN formation. Nematic gel samples with different gelator concentrations (1.0, 1.5 and 2.0 wt%) are first heated to 130 °C into the sol state. The samples are then rapidly quenched to T = 25 °C < T_{cl}. We recall that the lower limit of the two-phase region is at T_{cl} = 30 °C and after about 2 to 3 minutes, the N_C-phase is completely formed. The light intensity transmitted through the sample is measured without polarizers as a function of time. Looking at the sample with a gelator concentration of 1.5 wt% (green curve in Fig. 4), we see that the transmission remains constant for about 10 h and then decreases quite rapidly, later more slowly, to a saturation value which is not fully reached even after 50 h. We argue that the intensity is constant at the beginning because nuclei have to be formed first (nucleation period). Then the fibers begin to grow, and as they grow, the transmitted intensity begins to decrease. The light falling on the sample is scattered by the gel fibers, causing the sample to appear increasingly cloudy. However, as gel formation progresses, the liquid phase becomes increasingly immobilized, which in turn makes mass transport more difficult and slows further fiber growth. At a higher gelator concentration of 2.0 wt% (blue curve in Fig. 4), the nucleation period is shortened and the subsequent drop in transmission is much faster. Obviously, the formation of the gel network is complete after about 30 h and thus proceeds on the same time scale as the coarsening of the nematic domains. At a lower gelator concentration of 1.0 wt% (red curve in Fig. 4), there is no significant drop in transmission even after 60 h. The gelator concentration is so low that it takes days for a gel network to form.

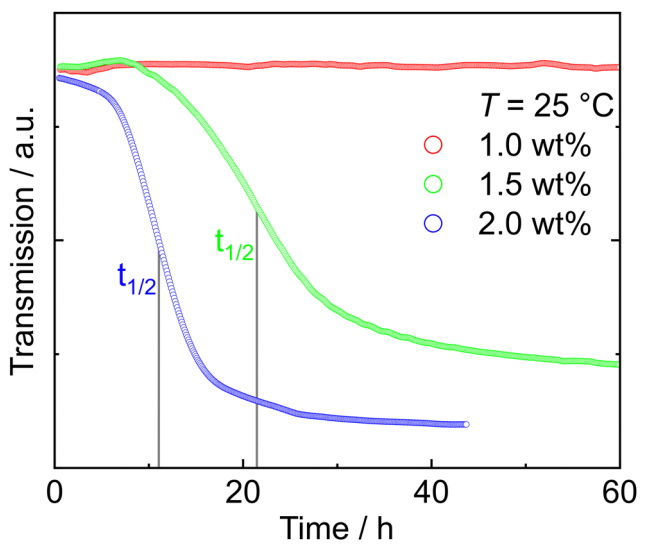

Fig. 4 Kinetics of gel formation as monitored by measurements of gel sample transmission (without polarizers) over time. At time t_0 = 0 h, samples with three different gelator concentrations were quenched from the sol state at 130 °C to room temperature. As a result of the light scattering at the growing network, the transmitted light intensity decreases and approaches a lower stationary limit when the network formation is complete. The halftime of the decay in transmission depends on the gelator concentration. At 1.0 wt% of gelator, no network formation is observed within 60 h.

From the results shown in Fig. 4, we conclude that for the subsequent experiments on the macroscopic alignment of nematic gels, it is best to choose a gelator concentration of about 1.5 wt%, since this provides a time window of a few hours between the appearance of the nematic phase and the formation of the gel network. This time window may be sufficient to align the nematic phase in an external magnetic field before the gel network is formed.

3.2. Macroscopic alignment of nematic gels

In general, the N_C-phase has a positive magnetic anisotropy $\Delta\chi = \chi_{\parallel} - \chi_{\perp} > 0$ with a magnetic susceptibility $\chi_{\parallel}$ that is larger in the direction parallel to the director n of the rod-like micelles than the susceptibility $\chi_{\perp}$ perpendicular to n. As a result, a magnetic field B aligns the director of the N_C-phase parallel to B, provided that the re-alignment of the N_C-phase is not hindered by other factors, such as the presence of a gel network.

According to the results from Section 3.1, a nematic gel with a gelator concentration of 1.5 wt% was chosen and sealed in a flat capillary. The sample is not aligned and has a polydomain texture. Then the sample is heated into the isotropic sol state at T = 130 °C and held at this temperature for three minutes. Afterwards, it is placed in the magnetic field and quenched to T = 25 °C. The magnetic field points along the long axis of the capillary (Fig. 5(a)). Gel formation is complete after hours to days. The sample capillary is removed from the magnetic field and examined using polarized optical microscopy (POM).

Looking at Fig. 5(b), one sees that it was indeed possible to align the director n of the nematic gel parallel to the magnetic field **B** and thus parallel to the long capillary axis. If the polarizer P and the analyzer A in Fig. 5(b) are at an angle of ±45° to n, the sample has maximum brightness (bright position), while if P and A are parallel and perpendicular to n, the sample has maximum darkness (dark position). As Fig. 5(c) shows, an alignment is not only found at selected spots of the sample, but uniformly over the entire capillary. This means that we have actually succeeded in producing centimeter-long sample films of a uniformly aligned nematic hydrogel! These films measure 3 cm in length, 0.3 cm in width, and 0.3 mm in height.

However, it is striking that the textures in Fig. 5(b) and (c), in particular those in the bright positions, have a stripe pattern parallel to n which might be caused by gel fibers that run parallel to n in an ordered manner. In fact, individual fibers (about 40 nm in diameter) cannot be resolved with an optical microscope, but it is possible that the fibers are clustered into so-called fiber bundles.[43] This does not destroy the gel network and the bundles can reach diameters of up to 1 μm, which, in turn, might be seen using POM. A second scenario is that a fiber may elastically deform the director field of the surrounding nematic phase. Local elastic deformations decay over the length scale known as the elastic coherence length, which is typically in the range of a few micrometers and is therefore also resolvable in the polarized optical microscope.

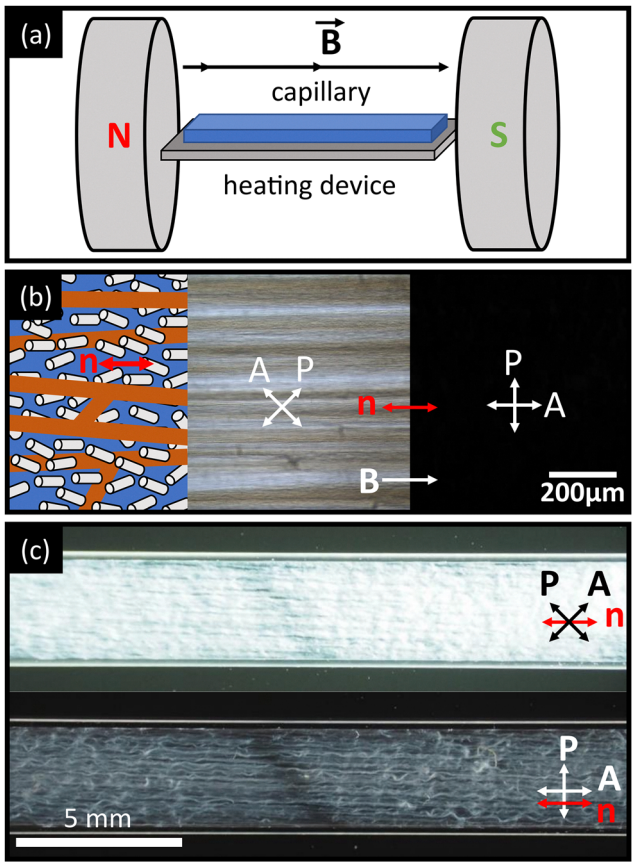

Fig. 5 (a) Schematic illustration of the magnetic-field alignment setup. (b) Schematic illustration of magnetic-field aligned sample with corresponding POM images of a real nematic hydrogel sample with aligned director *n* in the bright and in the dark positions of polarizer P and crossed analyzer A. (c) Same as (b) but now showing the entire capillary in a stereo microscope.

In any case, it appears that the aligned N_C-phase acts as a template, such that the fibers exhibit a preferential (though not exclusive) growth along *n*, resulting in the formation of a partially ordered gel network with anisotropic topology. It has been previously demonstrated that such template effects exist in the case of thermotropic LCs,[44] and thus it may be expected that they also occur with lyotropic LCs.[17] Furthermore, the anisotropic gel network appears to also exhibit a template or memory-effect, such that it remembers and maintains the alignment of the N_C-phase originally imprinted by the magnetic field. Once aligned, the nematic gels retain their alignment even after months outside the magnetic field, provided that the gel network is not destroyed. The next Section will examine this interesting memory-effect of the gel network in more detail.

3.3. Memory-effect in aligned nematic gels

To further study the potential memory-effect of the aligned nematic gel, the temperature program shown in Fig. 6 was applied. First, the sample was prepared and aligned using the quenching procedure from (0) to (1) as described in Section 3.2 under the action of an external magnetic field with B = 1 T. Subsequently, the external magnetic field was turned off for all following steps from (1) to (5) of the experiment. The aligned nematic gel at room temperature (1) was heated to T = 40 °C (2) to complete a phase transition from the nematic to the isotropic phase (T_{cl} = 34.2 °C). The sample remains below the sol–gel transition temperature (T_{sg} = 55 °C) such that the gel network remains unaffected. The isotropic gel was then cooled to room temperature (3) to reform the nematic phase. The nematic gel was then heated to T = 130 °C (4), causing both a phase transition from the nematic phase to the isotropic phase and a melting of the gel network. Finally, the sample was cooled to room temperature (5) to allow the nematic phase and gel network to reform. After each step of the temperature program, images of the samples were recorded under a microscope with and without crossed polarizers. For the images taken with crossed polarizers two positions were chosen, one in the bright position of the aligned sample and one in its dark position, in order to check the state of alignment during the different stages of the experiment.

The microscopy images (a–c) as well as schematic drawings (d) of each stage (1–5) of the experiment described in Fig. 6 are shown in Fig. 7. The samples between crossed polarizers can be seen in (a) the bright position and (b) the dark position. For the

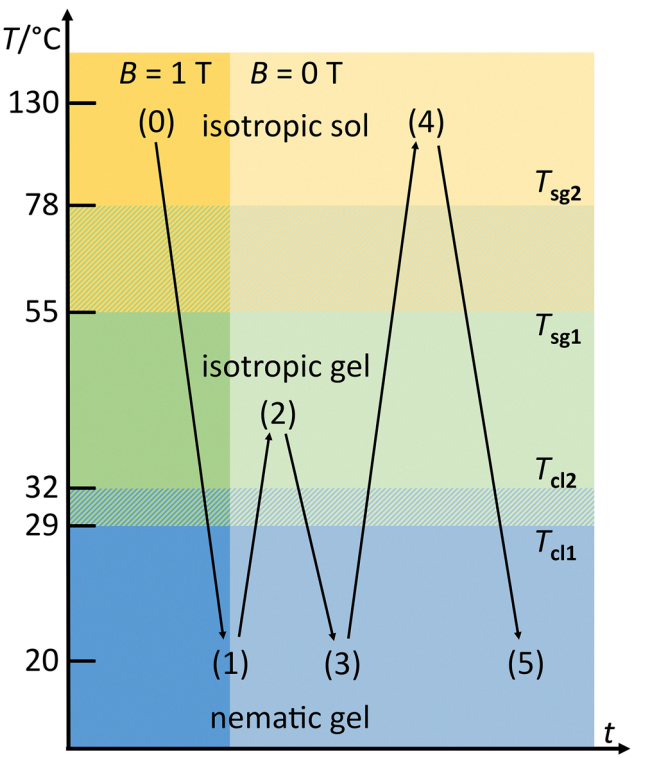

Fig. 6 Temperature program to study templating- and memory-effects between LLC and SAFIN. Initially, the sample was magnetically aligned at B = 1 T during quenching from (0) to (1) (see Section 3.2). The magnetic field was then removed for all subsequent stages. The nematic gel (1) is heated above the clearing temperature range T_{cl} to transfer the nematic into an isotropic phase while the gel network is conserved (2). Cooling back into the nematic gel state (3) and (4) heating above the sol–gel temperature range T_{sg} into an isotropic sol. Cooling again into the nematic gel state (5).

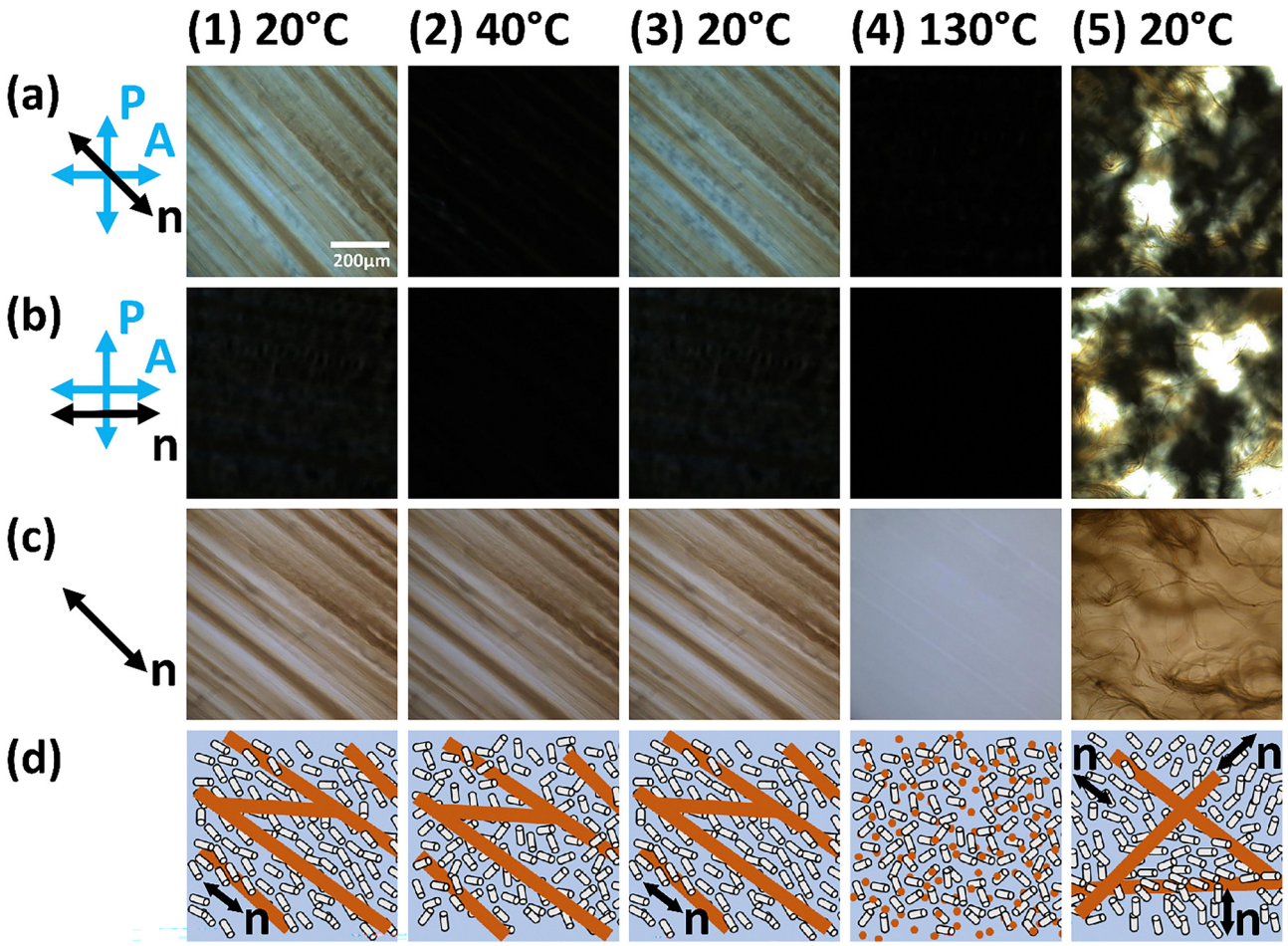

Fig. 7 Results of the experiment shown in Fig. 6. POM pictures of an aligned nematic gel. The macroscopically aligned nematic gel is shown in bright (a) and dark (b) positions with respect to the crossed polarizers. The comparison between the bright and dark positions provides information about the quality of the alignment of the sample. In row (c) the sample is shown without polarizers to visualize only the gel network. In row (d) the respective arrangements of micelles and gel fibers are schematically scetched. The aligned nematic gel (1) is heated above the clearing temperature (2), while the gel network is conserved ($T_{sg} > T_{cl}$), resulting in an isotropic gel. After cooling the nematic phase has the same alignment as before (3). This memory-effect is based on the aligned gel network. Heating the nematic gel to an isotropic sol (4) and cooling down (5) again, no memory-effect can be observed afterwards.

third row (c) the crossed polarizers were removed and only the gel network remains visible. A schematic drawing representing the anticipated structure of the sample in each stage of the experiment was added in the fourth row (d) which shows the micelles (grey) and water (blue) as well as the topology of the network (brown). In the first column (1) the initial alignment of the nematic phase (a1, b1) and the gel network (c1) are shown. Comparing the bright (a1) and dark (b1) position, one sees the macroscopic alignment of the nematic phase. Analogous to the nematic phase, the alignment of the gel network (c1) can be observed, which possesses the same preferred direction as the nematic phase. The second column (2) shows the sample after having been heated to $T = 40$ °C. The bright (a2) and dark (b2) position between crossed polarizers are both black, showing a phase transition from the nematic phase to the isotropic phase and the loss of the alignment. The gel network (c2), however retains the alignment after the heating. In the third column (3) the sample was cooled to room temperature and the nematic phase was reformed. The bright (a3) and dark (b3) position between crossed polarizers is virtually indistinguishable from (1) and the nematic phase follows the same director as the gel network (c3) which has remained unchanged. The fourth column (4) shows the sample at $T = 130$ °C with both bright (a4) and dark (b4) position being black and the gel network (c4) being completely dissolved. In the fifth and final column (5) the initially bright (a5) and dark (b5) positions show no significant difference with both containing bright and dark spots indicating multiple polydomains as opposed to an overall alignment. The gel network (c5), likewise, reforms without a preferred direction. Schematic drawing of the individual stages of the experiment are shown in the fourth row (d). It must be noted that over the course of this experiment no external stimuli that (re)aligns the nematic phase were applied. As such the driving force for the realignment must be the gel network which provides a sort of ''memory'' that allows the nematic phase to reform in its original orientation. Importantly, the heating cycle

(1–3) can be repeated three times without a significant loss of the orientation of the nematic phase (Fig. SI1). This memory-effect works similarly to the templating effect of the nematic phase on the gel network. As described in Section 3.2, after cooling from an isotropic sol the nematic phase forms first and can be aligned with a magnetic field. This aligned nematic phase then works as a template allowing the gel network to be aligned alongside the same director as the nematic phase. The aligned gel network can then, in turn, induce the aligned formation of the nematic phase from the isotropic phase (1–3) along its director as long as the sample is not heated above the sol–gel transition temperature (T_{sg} = 55 °C) where the gel starts to dissolve and loses its memory-effect.

To determine whether this memory-effect is a general phenomenon of nematic gels, the experiment was repeated using the ternary system H_2O – *N*,*N*,*N*-trimethyl-1-tetradecylammonium bromide (C_{14}TAB) – *n*-decanol. The results are shown in Fig. SI2. We found that the ternary system behaves similarly to the binary system, with a memory-effect being observable as long as the T_{sg} was not crossed. However, noticeable differences were observed as regards the initial alignment of the gel network (1) as well as the formation time of the nematic phase after cooling from T = 130 °C (5). As regards the gel network formation, the gel network of the ternary system does not align as neatly as the binary system under the same conditions. This is due to the fact that the nematic phase of the ternary system forms much slower than that of the binary system due to the delayed incorporation of the cosurfactant as discussed in ref. 45. The formation of the N_C-phase of the ternary system takes up to 3 hours, whereas the formation of the N_C-phase of the binary system requires merely 1 minute.[45] The long formation of the N_C-phase disturbs the templating process as the gel network can grow randomly until the nematic phase forms. The nematic phase only acts as a template for the gel formation if it is aligned. In summary, the aligned nematic gels of both the binary and ternary system have a memory-effect causing the nematic phase to align along the director of the gel network.

4. Conclusions

The key result of this work is that centimeter-long sample films of macroscopically aligned nematic gels can be generated by growing a self-assembling fiber gel network in a magnetically aligned lyotropic nematic N_C-phase. After the gel network is completely formed, the macroscopic alignment of the nematic phase is preserved even in the absence of a magnetic field and is recovered even after melting and reformation of the N_C-phase.

These remarkable alignment- and memory-effects are apparently the result of the interplay between lyotropic liquid crystalline order and gel network topology: On the one hand, the macroscopically aligned nematic matrix acts as an effective template that directs fiber growth, ultimately resulting in an overall anisotropic gel network. On the other hand, the anisotropic gel network acts as a kind of "memory" of the system, such that the original alignment of the nematic phase is maintained in the absence of a magnetic field and is recovered after melting and reformation of the N_C-phase.

The recovery of the aligned nematic phase is currently only verified using polarized optical microscopy (POM), and the alignment of the gel network is only suspected, as some samples visually show a preferred direction of the fibers. To unambiguously confirm the templating-effect of the LLC on the anisotropy of the gel network and, in turn, the memory-effect of the anisotropic gel network on the LLC, we have recently undertaken small-angle neutron scattering experiments, including contrast variations that allow the gel network and the LLC to be studied selectively. These experiments will be presented and discussed in a follow-up publication.

We are confident that this simple and robust method for preparing macroscopically aligned anisotropic hydrogels is an important step towards their use in, *e.g.*, biomedical applications.

Conflicts of interest

The authors declare no conflicts of interest.

Data availability

SI with data from another micellar lyotropic system available. Additional data available upon request.

Supplementary information is available. See DOI: **https://doi.org/10.1039/d5tc01659b**

Acknowledgements

We thank Natalie Preisig for carrying out the FFEM investigations. This research was supported by the Deutsche Forschungsgemeinschaft (grants DFG GI 243/9-2 and DFG STU 287/6-2).

Notes and references

1 E. S. Wu, K. Jacobson and D. Papahadjopoulos, Lateral diffusion in phospholipid multibilayers measured by fluorescence recovery after photobleaching, *Biochemistry*, 1977, **16**, 3936–3941.
2 P. F. Fahey and W. W. Webb, Lateral diffusion in phospholipid bilayer membranes and multilamellar liquid crystals, *Biochemistry*, 1978, **17**, 3046–3053.
3 C. Honorato-Rios, C. Lehr, C. Schütz, R. Sanctuary, M. A. Osipov, J. Baller and J. P. F. Lagerwall, Fractionation of cellulose nanocrystals: enhancing liquid crystal ordering without promoting gelation, *NPG Asia Mater.*, 2018, **10**, 455–465.
4 J. R. Bruckner, A. Kuhnhold, C. Honorato-Rios, T. Schilling and J. P. F. Lagerwall, Enhancing Self-Assembly in Cellulose Nanocrystal Suspensions Using High-Permittivity Solvents, *Langmuir*, 2016, **32**, 9854–9862.
5 M. Nordenström, A. Fall, G. Nyström and L. Wågberg, Formation of Colloidal Nanocellulose Glasses and Gels, *Langmuir*, 2017, **33**, 9772–9780.

6 P. Davidson, C. Bourgaux, L. Schoutteten, P. Sergot, C. Williams and J. Livage, A Structural Study of the Lyotropic Nematic Phase of Vanadium Pentoxide Gels, *J. Phys. II France*, 1995, **5**, 1577–1596.
7 C. Stubenrauch and F. Gießelmann, Gelled Complex Fluids: Combining Unique Structures with Mechanical Stability, *Angew. Chem., Int. Ed.*, 2016, **55**, 3268–3275.
8 K. Steck, S. Dieterich, C. Stubenrauch and F. Giesselmann, Surfactant-based lyotropic liquid crystal gels – the interplay between anisotropic order and gel formation, *J. Mater. Chem. C*, 2020, **8**, 5335–5348.
9 E. R. Draper and D. J. Adams, Low-Molecular-Weight Gels: The State of the Art, *Chem*, 2017, **3**, 390–410.
10 C. D. Jones and J. W. Steed, Gels with sense: supramolecular materials that respond to heat, light and sound, *Chem. Soc. Rev.*, 2016, **45**, 6546–6596.
11 F. M. Menger, Y. Yamasaki, K. K. Catlin and T. Nishimi, X-Ray Structure of a Self-Assembled Gelating Fiber, *Angew. Chem., Int. Ed. Engl.*, 1995, **34**, 585–586.
12 R. G. Weiss, *Molecular Gels. Materials with Self-Assembled Fibrillar Networks*, Springer, Netherlands, Dordrecht, 1st edn, 2006.
13 R. G. Weiss, The past, present, and future of molecular gels. What is the status of the field, and where is it going?, *J. Am. Chem. Soc.*, 2014, **136**, 7519–7530.
14 D. K. Smith, Supramolecular gels – a panorama of low-molecular-weight gelators from ancient origins to next-generation technologies, *Soft Matter*, 2023, **20**, 10–70.
15 P. Terech and R. G. Weiss, Low Molecular Mass Gelators of Organic Liquids and the Properties of Their Gels, *Chem. Rev.*, 1997, **97**, 3133–3160.
16 D. J. Abdallah and R. G. Weiss, Organogels and Low Molecular Mass Organic Gelators, *Adv. Mater.*, 2000, **12**, 1237–1247.
17 S. Dieterich, F. Stemmler, N. Preisig and F. Giesselmann, Micellar Lyotropic Nematic Gels, *Adv. Mater.*, 2021, **33**, e2007340.
18 K. Sano, Y. Ishida and T. Aida, Synthesis of Anisotropic Hydrogels and Their Applications, *Angew. Chem., Int. Ed.*, 2018, **57**, 2532–2543.
19 *Molecular Biology of the Cell*, ed. B. Alberts, A. Johnson, J. Lewis, M. Raff, K. Roberts and P. Walter, Garland Science, 4th edn, 2002.
20 J. F. Douglas, Weak and Strong Gels and the Emergence of the Amorphous Solid State, *Gels*, 2018, **4**(1), 1–14.
21 A. Aggeli, M. Bell, L. M. Carrick, C. W. G. Fishwick, R. Harding, P. J. Mawer, S. E. Radford, A. E. Strong and N. Boden, pH as a trigger of peptide beta-sheet self-assembly and reversible switching between nematic and isotropic phases, *J. Am. Chem. Soc.*, 2003, **125**, 9619–9628.
22 J.-L. Pozzo, G. M. Clavier and J.-P. Desvergne, Rational design of new acid-sensitive organogelators, *J. Mater. Chem.*, 1998, **8**, 2575–2577.
23 T. Kato, Self-Assembly of Phase-Segregated Liquid Crystal Structures, *Science*, 2002, **295**, 2414–2418.
24 C. Ohm, M. Brehmer and R. Zentel, Liquid crystalline elastomers as actuators and sensors, *Adv. Mater.*, 2010, **22**, 3366–3387.
25 K. M. Herbert, H. E. Fowler, J. M. McCracken, K. R. Schlafmann, J. A. Koch and T. J. White, Synthesis and alignment of liquid crystalline elastomers, *Nat. Rev. Mater.*, 2022, **7**, 23–38.
26 T. J. White and D. J. Broer, Programmable and adaptive mechanics with liquid crystal polymer networks and elastomers, *Nat. Mater.*, 2015, **14**, 1087–1098.
27 H. Wermter and H. Finkelmann, Liquid crystalline elastomers as artificial muscles, *e-Polymers*, 2001, **1**(13), 1–13.
28 I. Dierking, *Polymer-modified Liquid Crystals*, Royal Society of Chemistry, Cambridge, 1st edn, 2019.
29 P. J. Collings and J. W. Goodby, Introduction to liquid crystals, *Chemistry and physics*, CRC Press Taylor & Francis Group, Boca Raton, FL, 2020.
30 F. Y. Fujiwara and L. W. Reeves, Liquid crystal/glass interface effects on the orientation of lyotropic liquid crystals in magnetic fields, *Can. J. Chem.*, 1978, **56**, 2178–2183.
31 U. Kaeder and K. Hiltrop, Alignment of lyotropic nematics by surface action, *Trends in Colloid and Interface Science V*, 1991, vol. 84, pp. 250–252.
32 C. F. Dietrich, P. J. Collings, T. Sottmann, P. Rudquist and F. Giesselmann, Extremely small twist elastic constants in lyotropic nematic liquid crystals, *Proc. Natl. Acad. Sci. U. S. A.*, 2020, **117**, 27238–27244.
33 S. Dieterich, T. Sottmann and F. Giesselmann, Gelation of Lyotropic Liquid-Crystal Phases-The Interplay between Liquid Crystalline Order and Physical Gel Formation, *Langmuir*, 2019, **35**, 16793–16802.
34 F. Schörg, PhD thesis, Universität Stuttgart, 2015.
35 M. Laupheimer, N. Preisig and C. Stubenrauch, The molecular organogel n-decane/12-hydroxyoctadecanoic acid: Sol–gel transition, rheology, and microstructure, *Langmuir*, 2015, **469**, 315–325.
36 M. Herbst, M. O. Dombrowski, N. Preisig, S. Dieterich, F. Giesselmann, P. Mésini and C. Stubenrauch, Gelled lyotropic nematic liquid crystals, *Liq. Cryst.*, 2023, **50**, 1090–1100.
37 N. Díaz, F.-X. Simon, M. Schmutz, M. Rawiso, G. Decher, J. Jestin and P. J. Mésini, Self-Assembled Diamide Nanotubes in Organic Solvents, *Angew. Chem., Int. Ed.*, 2005, **117**, 3324–3328.
38 A. Jamal, I. Nyrkova, P. Mesini, S. Militzer and G. Reiter, Solvent-controlled reversible switching between adsorbed self-assembled nanoribbons and nanotubes, *Nanoscale*, 2017, **9**, 3293–3303.
39 F.-X. Simon, T. T. T. Nguyen, N. Díaz, M. Schmutz, B. Demé, J. Jestin, J. Combet and P. J. Mésini, Self-assembling properties of a series of homologous ester-diamides – from ribbons to nanotubes, *Soft Matter*, 2013, **9**, 8483.
40 A. Saipa and F. Giesselmann, A high resolution temperature scanning technique for optical studies of liquid crystal phase transitions, *Liq. Cryst.*, 2002, **29**, 347–353.
41 E. Akpinar, E. Guner, O. Demir-Ordu and A. M. F. Neto, Effect of head-group size of some tetradecylalkylammonium bromide surfactants on obtaining the lyotropic biaxial nematic phase, *Eur. Phys. J. E*, 2019, **42**, 44.
42 Y. Galerne and J. P. Marcerou, Temperature Behavior of the Order-Parameter Invariants in the Uniaxial and Biaxial

Nematic Phases of a Lyotropic Liquid Crystal, *Phys. Rev. Lett.*, 1983, **51**, 2109–2111.

43 D. Schwaller, S. Zapién-Castillo, A. Carvalho, J. Combet, D. Collin, L. Jacomine, P. Kékicheff, B. Heinrich, J.-P. Lamps, N. P. Díaz-Zavala and P. J. Mésini, Gel-to-gel non-variant transition of an organogel caused by polymorphism from nanotubes to crystallites, *Soft Matter*, 2021, **17**, 4386–4394.

44 T. Kato, Y. Hirai, S. Nakaso and M. Moriyama, Liquid-crystalline physical gels, *Chem. Soc. Rev.*, 2007, **36**, 1857–1867.

45 M. Dombrowski, M. Herbst, N. Preisig, F. Giesselmann and C. Stubenrauch, Time Dependence of Gel Formation in Lyotropic Nematic Liquid Crystals: From Hours to Weeks, *Gels*, 2024, **10**, 261.